MMSE Receivers for Multirate DS-CDMA Systems

Ashutosh Sabharwal, *Member, IEEE*, Urbashi Mitra, and Randolph Moses, *Senior Member, IEEE*

***Abstract*—Minimum-mean squared error (MMSE) receivers are designed and analyzed for multiple data rate direct-sequence code-division multiple-access (DS-CDMA) systems. The inherent cyclostationarity of the DS-CDMA signal is exploited to construct receivers for asynchronous multipath channels. Multiple- and single-bandwidth access are treated for both single and multicarrier scenarios. In general, the optimal receiver is periodically time-varying. When the period of the optimal receiver is large, suboptimal receivers are proposed to achieve a lower complexity implementation; the receivers are designed as a function of the cyclic statistics of the signals. In multiple chipping rate systems, complexity of receivers for smaller bandwidth users can also be controlled by changing their front-end filter bandwidth. The effect of front-end filter bandwidth on receiver performance and system capacity is quantified for a variable chipping rate system. Analysis and simulation show that significant performance gains are realized by the periodically time-varying MMSE receivers over their time-invariant counterparts.**

***Index Terms*—Asynchronous DS-CDMA, cyclostationarity, multicarrier systems, multipath channels, multimedia systems, multiple data rate, MMSE receivers.**

I. Introduction

DIRECT-SEQUENCE code division multiple access (DS-CDMA) has emerged as a promising technique for providing multi-user access in outdoor wireless systems. Past efforts to create robust and efficient receivers for DS-CDMA communication had been driven by the current cellular telephony network and thus focused on constant bit-rate traffic such as voice, e.g., [1], [2]. With the exploding growth of cellular communication systems, there has been a considerable interest in providing wireless transport for a variety of data sources, including images (facsimiles), video, data, and voice. To serve sources with inherently different information rates in a wireless system, it is desirable to develop systems that operate at multiple data rates. This paper considers receiver design for DS-CDMA systems which allow multiple data rate access.

Early work on DS-CDMA multirate systems focused on resource allocation [3], [4], rather than on receiver design; the use of the conventional receiver predominated. Recent attention has been directed toward the development of DS-CDMA receivers for multirate systems. Among the receivers proposed for multirate DS-CDMA systems are the conventional receiver [3], [4], decorrelator-based receivers [5], [6], minimum-mean-squared error (MMSE) receivers [7], the optimum receiver [8], and receivers based on successive interference cancellation [9]. Much of the prior work on multirate receiver design assumed a constant chipping rate, with multirate access being achieved by varying the spreading gain or by multiplexing the high rate traffic.

If one synthesizes the recent work in the development of multirate receiver design, an interesting dichotomy appears. Receivers that truly exploit the nature of multirate signals have focused on synchronous and pseudosynchronous systems [6], [8]. Designs which accommodate asynchronous or multipath channels [7] do not take advantage of the multirate nature of the signals. In the current work, we seek to design practical receivers which can accommodate the distortion induced by the wireless channel while simultaneously exploiting the multirate nature of the signals.

Proposed third-generation DS-CDMA standards consider a variety of methods for accomplishing multiple data rates. Variable spreading length (constant chip-rate), multi-code, and discontinuous transmission schemes are discussed in [10] and [11] in reference to UMTS/IMT2000 and W-CDMA. In [11], multiple chip rates are also specified for the radio link. It is anticipated that future standards will incorporate hybrid versions of the different multirate access schemes to tailor the data rate to the application.

The current work is informed by past research on the development of rate-separation filters for multiple chip-rate systems. In [12], we examined the feasibility of preprocessing the received signal into multiple single data-rate signals. The filtering operation was followed by modified single-rate receivers. Filtering improved performance over matched filtering, but only marginal improvements were seen for low rate users. The reasons for limited gain of the rate-separating filters will be explained in the sequel.

Our objective is to design and analyze MMSE receivers for multirate DS-CDMA signals transmitted over asynchronous, multipath channels. Our contributions can be summarized as follows.

- We use the inherent cyclostationarity of the multirate signal to construct the optimal MMSE receiver. It is shown that, in the presence of multirate interference, the optimal MMSE receiver can be periodically time-varying. The optimal MMSE receiver is derived both in the time and frequency domains. In the time domain, the original

Paper approved for publication by G. Caire, the Editor for Multiuser Detection and CDMA of the IEEE Communications Society. Manuscript received March 15, 2000; revised May 15, 2001. This work was supported in part by an Ameritech Dissertation Fellowship and in part by the National Science Foundation under CAREER Grant NCR 96-24375. This paper was presented in part at the 34th Annual Conference on Information Sciences and Systems, Princeton, NJ, March 2000, and at the IEEE Wireless Communications and Networking Conference, New Orleans, LA, September 1999.

A. Sabharwal is with the Department of Electrical and Computer Engineering, Rice University, Houston, TX 77005 USA.

U. Mitra is with the Department of Electrical Engineering, University of Southern California, Los Angeles, CA 90089 USA (e-mail: ubli@usc.edu).

R. Moses is with the Department of Electrical Engineering, The Ohio State University, Columbus, OH 43210 USA.

Publisher Item Identifier S 0090-6778(01)10605-7.

problem is mapped to a set of decoupled single-rate (virtual user) problems, which clearly demonstrates the periodic nature of the optimal solution. In the frequency domain, the filter coefficients are shown to satisfy a set of linear equations, which can be understood as a multichannel extension of a single-rate MMSE receiver.

- The periodicity of the optimal MMSE receiver is exploited to design low-complexity suboptimal MMSE receivers. The periodic MMSE receiver admits a discrete Fourier series expansion, which is pruned to obtain different low-complexity receivers. Though the suboptimal receiver does not admit a decoupling as the optimal receiver, our derivations show that it can be obtained by deleting certain rows and columns from the set of linear equations for the optimal receiver. Based on the mean-squared error analysis, a heuristic method for the choice of best suboptimal receiver is also proposed.
- We study the effect of front-end filter bandwidth in multiple bandwidth systems, which quantifies the performance complexity tradeoff for lower bandwidth users in multiple bandwidth systems.

The proposed framework is applicable to DS-CDMA systems with multiple spreading gains, multiple chipping rates, and multicarrier transmission[1] in the presence of multipath. The MMSE receivers are derived without any causality constraints; this extends the work in [14] and [15] to data demodulation for multirate signals. The primary motivation for not imposing causality constraints is to learn the structure of optimal MMSE receivers and use it as a precursor to practical adaptive and blind causal implementations.

The motivation for seeking low-complexity receivers comes from the range of proposed data rates in the next generation systems, from tens of kilobits per second to roughly 2 Mb/s [10]. The complexity of linear MMSE receivers in future systems with variable symbol periods will be governed by two major factors: periodicity of the receiver, and length of the receiver. For large-periodicity optimal receivers, we derive low complexity suboptimal MMSE receivers. The suboptimal MMSE receivers, of which the time-invariant MMSE receiver is a special case, can offer near-optimal performance in some cases. The length of the receivers depends on the sampling rate, or equivalently, on the front-end filter bandwidth. Thus, we study the effect of the front-end filter bandwidth to quantify the complexity-performance tradeoff.

Cyclostationary signals with multiple periodicities have been extensively studied in ([16] and references therein) and the concepts have been extensively used in communications, e.g., in cyclic signal separation [16], system identification [16], [17], and synchronization [16]. The results in this paper are in the same spirit as cyclic Wiener filtering [16], but differ in one key aspect. We consider data demodulation instead of estimating the complete modulated signal as in [16]; the two problems are different if the signaling bandwidth is more than the information rate as is the case in DS-CDMA.

In concept, our paper shares much with that of [18], though both works were done independently. Both works exploit the inherently cyclostationarity of the multirate receiver to design MMSE receivers. In [18], an approximate discrete time representation of an infinite bandwidth system (with square pulses) was used. Our derivation in continuous time requires no discrete time approximations and applies to arbitrary bandwidth systems. Both in [18] and this paper, truncation of discrete Fourier series of the optimal receiver is used to obtain low-complexity receivers; a time-domain approach is used in [18]. Our derivation of suboptimal receivers in the frequency domain leads to an important result that the zeroth Fourier coefficient, corresponding to the time-invariant MMSE receiver, should always be included to derive low-complexity MMSE receivers. In addition, we consider systematic methods for reducing complexity of the complete MMSE receiver while maintaining near-optimal performance. Finally, the consideration of band-limited signaling enables our discussion on the effects of front-end filter bandwidth.

This paper is organized as follows. In Section II, we formulate the problem and review the cyclostationarity of DS-CDMA signals. In Section III, we derive the optimal MMSE receiver and its Fourier coefficients. We derive suboptimal, low-complexity receivers in Section IV. The mean-squared error is also computed in Section IV, and the issue of choosing among low-complexity receivers is investigated. In Section V, we discuss the effect of the front-end filter bandwidth on system capacity in multiple-bandwidth systems. The performance of the proposed receivers is studied via simulations in Section VI, and conclusions are presented in Section VII. Appendix A provides representations of key matrices. In Appendix B, the reduced complexity receiver is derived.

II. Problem Formulation

In this section, we first define the multirate DS-CDMA signal model used in this paper. We also briefly review wide-sense cyclostationary stochastic processes and some of their properties, which are used throughout the paper.

A. Signal Model

For simplicity of presentation, we assume that all users employ the same carrier frequency; multicarrier systems are considered in [19]. The methods considered in the current work are applicable to multiple carrier systems without any modification.

The received baseband signal is

$$y(t) = \sum_{k=1}^{C} \sum_{i=1}^{P_k} A_{ik} x_{ik}(t) + \eta(t) \tag{1}$$

where

$$x_{ik}(t) = \sum_{l=-\infty}^{\infty} b_{ik}(l) s_{ik}(t - lT_k - \tau_{ik}). \tag{2}$$

[1]Narrow-band interference suppression is a special case of multicarrier transmission. Typically, the narrow-band data interferer is modeled as a stationary interferer (see [13] and references therein), which leads to a loss in performance as can be concluded from the results in this paper.

The number of service classes is denoted by C; each class corresponds to a different symbol period. There are P_k users in Class k. Each user in a particular class transmits at the same symbol rate, $(1/T_k)$, with spreading gain[2] L_k and chipping period $T_{c_k} = T_k/L_k$. Users are indexed by two variables: k indicates the class and i indicates the user number within Class k. The received signal for user ik is denoted by $x_{ik}(t)$. The corresponding received amplitude is A_{ik}. Each user ik is received after a propagation delay of τ_{ik}. The additive noise process, $\eta(t)$, is assumed to be white and stationary with zero mean and power $(N_o/2)$. The information stream for user ik is denoted by $b_{ik}(l)$ and $\mathbb{E}\{|b_{ik}(l)|^2\} = 1$. For simplicity of presentation, BPSK modulation is assumed. The information bits are assumed to be independent from user to user and in time. The effective spreading waveform is denoted by $s_{ik}(t)$ and is the convolution of the multipath, $m_{ik}(t)$, and the actual spreading waveform; the actual spreading waveform is formed by modulating a pseudorandom noise sequence, $a_{ik}(n)$, with the pulse shape $\phi_k(t)$

$$s_{ik}(t) = \underbrace{m_{ik}(t)}_{\text{multipath}} \circledast \underbrace{\sum_{n=1}^{L_{ik}} a_{ik}(n)\phi_{ik}\left(t - nT_{c_{ik}}\right)}_{\text{actual spreading waveform}}$$

such that $\| \sum_{n=1}^{L_{ik}} a_{ik}(n)\phi_k(t - nT_{c_{ik}})\| = 1$. The convolution operator is denoted by $\circledast$. Arbitrary pulse shapes $\phi_k(t)$ are considered herein, but in practice band-limited pulses are used.[3]

B. Cyclostationarity of the DS-CDMA Signal

We first investigate the second-order statistics of a single spread spectrum signal in the absence of noise. Consider the DS-CDMA signal, $x(t) = A\sum_l b(l)s(t - lT)$, with symbol period T and spreading gain L, where $s(t)$ is the symbol waveform. Due to the assumption of equally probable and independent data bits, $\mathbb{E}\{x(t)\} = 0$. Thus, the covariance function of $x(t), R_x(t,u)$, is

$$\begin{aligned} R_x(t,u) &= \mathbb{E}\left\{A\sum_{l=-\infty}^{\infty} b(l)s(t-lT)A\sum_{k=-\infty}^{\infty} b(k)s(u-kT)\right\} \\ &= A^2\sum_{l=-\infty}^{\infty}\sum_{k=-\infty}^{\infty}\mathbb{E}\{b(l)b(k)\}s(t-lT)s(u-kT) \\ &= A^2\sum_{n=-\infty}^{\infty} R_b(n)\sum_{l=-\infty}^{\infty} s(t-lT)s(u-lT-nT) \end{aligned}$$

where $R_b(n)$ is the correlation of the stationary data sequence. For i.i.d. data, $R_b(n) = \delta_n$, where the Kronecker delta function $\delta_n = 1$ if $n = 0$ and zero otherwise. Since $R_x(t,u) = R_x(t + kT, u + kT)\forall k$ is a periodic function of t and u with period T, its Fourier series expansion exists with fundamental frequency $1/T$. The harmonic frequencies in the Fourier series expansion of $R_x(t,u)$ are known as *cycle frequencies*. For the raised cosine pulse with a nonzero roll-off factor, only the coefficients corresponding to *cycle frequencies* $\{0, 1/T, \ldots, L/T\}$ are nonzero [16]. Let $X(f)$ denote the Fourier transform of $x(t)$ [20], then define $\Gamma_x(f,f') = \mathbb{E}\{X(f)X^*(f')\}$, where $X^*(f')$ is the complex conjugate of $X(f')$. If $R_x(t,u)$ is harmonizable [20], then $\Gamma_x(f,f')$ is the two-dimensional (2-D) Fourier transform of $R_x(t,u)$. Since $R_x(t,u)$ is periodic with period T, it implies that the following series representation exists for $\Gamma_x(f,f')$ [21]

$$\Gamma_x(f,f') = \frac{1}{T}\sum_{n=-\infty}^{\infty}\gamma_x^{(n)}(f)\delta\left(f - f' - \frac{n}{T}\right)$$

where $\gamma_x^{(n)}(f) = S(f)S^*(f - (n/T)), S(f)$ is the Fourier transform of $s(t)$ and $\delta(f)$ is the Dirac delta function. The cyclostationarity of $x(t)$ implies that the 2-D Fourier transform $\Gamma_x(f,f')$ is nonzero only along the diagonals $f = f' + n/T$.

Given the prior discussion, we can determine the autocorrelation of the received multirate signal $y(t)$ in (1) as

$$R_y(t,u) = \sum_{k=1}^{C}\sum_{i=1}^{P_k} A_{ik}^2 R_{ik}(t,u) + R_\eta(t-u) \qquad (3)$$

where $R_{ik}(t,u)$ is the covariance of $x_{ik}(t)$ and is periodic with period T_k. The covariance function of $\eta(t)$ is denoted by $R_\eta(t-u)$. The periodicity of $R_y(t,u)$ depends on the ratio of individual symbol periods T_k. For the rest of the paper, we assume there exists a finite T such that the ratio T/T_i is an integer for all $i = 1, \ldots, k$; assume that T is the smallest such integer. The period of $R_y(t,u)$ is T, i.e., $R_y(t+kT, u+kT) = R_y(t,u)\forall k$; the expression for $\Gamma_y(f,f')$ will be given in Section III. Finally, we define the constants, $v_k = (T/T_k)$; clearly, $v_k \in \mathbb{Z}^+$. In the next section, we will observe that the parameter v_k indicates the number of virtual users associated with user k present in duration T.

The results in the following sections are derived in the continuous time to allow infinite bandwidth systems [18]. Since the discrete time representation is more commonly used, the following results on cyclostationary processes [21] will clarify the results in the sequel. Consider an arbitrary cyclostationary process, $\nu(t)$, with a period of T seconds.

1) *Sampling*: If $\nu(t)$ is sampled every kT seconds, $k \in \mathbb{Z}^+$, then the sampled sequence, $\{\nu[n] = \nu(nkT)\}_{n=-\infty}^{\infty}$, is a stationary sequence.

   If $\nu(t)$ is sampled every T/k seconds, $k \in \mathbb{Z}^+$then $\{\nu[n] = \nu(nT/k)\}_{n=-\infty}^{\infty}$ is a cyclostationary sequence with period k. If we form the following vector process:

$$\nu[n] = [\nu[nk] \quad \nu[nk-1] \quad \cdots \quad \nu[nk-(k-1)]]^T$$

   then $\{\nu[n]\}_{n=-\infty}^{\infty}$ is a vector stationary process.
2) *Filtering*: Let $h(t)$ be a linear time-invariant filter, then $h(t) \circledast \nu(t)$ is cyclostationary with period T.

[2]User classes can be defined in several different ways. A class could constitute users with same bandwidth, which requires same chipping periods for the member users, with possibly different spreading gains for each user. For our purposes, class members will have the same symbol periods with possibly different chipping rates and hence different bandwidths; the reason for this choice will become evident in the next subsection.

[3]Rectangular pulse shapes and thus very wide bandwidth front-end filters are assumed in [18].

III. Optimal MMSE Receiver

In this section, we will derive the optimal linear MMSE receiver. Two equivalent formulations for the optimal receiver are given. The first derivation relies on decomposing each user into several virtual users [22] to convert the original problem into a single rate multiuser problem. This solution clearly demonstrates the cyclic time-variation of the optimal MMSE filter. Having established the periodic time-variation of the optimal receiver, we then determine the Fourier series expansion of the optimal receiver. The Fourier series expansion enables the development of lower complexity suboptimal receivers.

The desired linear receiver structure is shown in Fig. 1, where $h(t)$ is the front-end filter. We include $h(t)$ to facilitate the discussion of the effects of front-end filter bandwidth in Section V. The MMSE receiver, $u(t,l)$, is constrained to be linear, but no constraint on time-invariance or causality is imposed. Further, we consider symbol-by-symbol demodulation, i.e., symbol decisions are made at the end of each symbol.

A. Optimal MMSE Receiver

Without loss of generality, we consider user 1 in Class 1, i.e., user 11; the soft symbol estimates are obtained by sampling the output of a linear filter at $t = lT_1$

$$\hat{b}_{11}(l) = u_l(t) \circledast h(t) \circledast y(t)|_{t=lT_1} \tag{4}$$

where $u_l(t)$ is the linear receiver used to demodulate symbol $b_{11}(l)$. Actual bit estimates are obtained by hard limiting the soft estimates, $\hat{b}_{11}(l)$, to the closest symbol value. The objective is to minimize the mean-squared error between the true data symbols and their soft estimates

$$\{u_l^\circ(t)\}_{l=-\infty}^{\infty} = \arg \min_{\{u_l(t)\}_{l=-\infty}^{\infty}} \mathbb{E}_l \mathbb{E}_b \|b_{11}(l) - \hat{b}_{11}(l)\|^2 \tag{5}$$

where $\mathbb{E}_l$ is the time average, $\mathbb{E}_b$ is the ensemble average, and $\{u_l(t)\}_{l=-\infty}^{\infty}$ is the sequence of receivers for each symbol. The reason for introducing the time average, $\mathbb{E}_l$, is as follows. If the receiver, $u_l(t)$, for the lth symbol is optimized independently of the receivers for the other symbols, then the solution to (5) is same as that for the conventional MMSE problem ([2], [15] for the single-rate MMSE receiver)

$$u_l^\circ(t) = \arg \min_{u_l(t)} \mathbb{E}_b \|b_{11}(l) - \hat{b}_{11}(l)\|^2. \tag{6}$$

This can be concluded by observing

$$\begin{aligned} &\mathbb{E}_l \mathbb{E}_b \|b_{11}(l) - \hat{b}_{11}(l)\|^2 \\ &= \lim_{M\to\infty} \frac{1}{2M+1} \sum_{l=-M}^{M} \mathbb{E}_b \|b_{11}(l) - \hat{b}_{11}(l)\|^2 \end{aligned} \tag{7}$$

and that the first-order sufficient condition [23] (orthogonality) for the optimization problem (5) is identical to the condition for (6) (under the assumption that the limit in (7) converges uniformly). In contrast, if the receivers $\{u_l(t)\}$ are chosen from a constrained class of receivers, then the decoupled optimization in (6) cannot be used; instead, (5) should be used for a joint optimization. The joint optimization (5) will be used in Section IV to derive low-complexity suboptimal receivers.

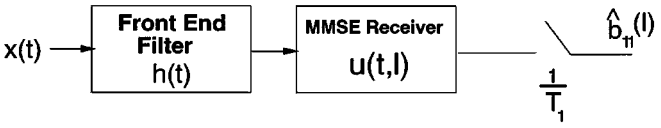

Fig. 1. Receiver structure.

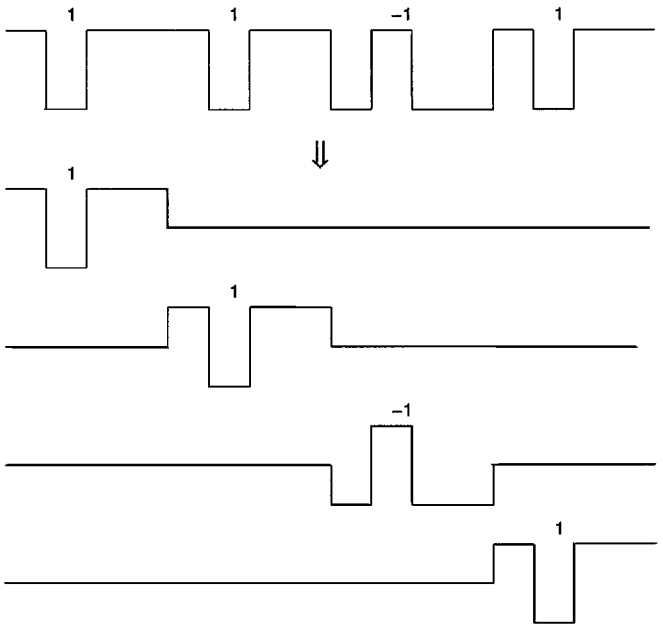

Fig. 2. Decomposition of a user into virtual users for the case of $v_1 = 4$. The labels on the signals represent the data bit values.

Thus, the optimal MMSE receiver $u_l^\circ(t)$ can be obtained as a solution to (6) and can be derived using the results in [2], [15]. Next we show that we need to solve the optimization problem (5) for only v_1 consecutive values of l.

Since the symbols for each user ik are uncorrelated, user ik's signal can be decomposed into v_k virtual users, each with symbol rate $T = v_k T_k$ (see Fig. 2). The received signal for user ik can thus be rewritten as

$$x_{ik}(t) = \sum_{d=0}^{v_k-1} \sum_{l=-\infty}^{\infty} b(lv_k + d) s_{ik}(t - (lv_k + d)T_k - \tau_{ik}). \tag{8}$$

Note that the original multirate problem has $\sum_{k=1}^{C} P_k$ users and is equivalent to a single rate problem with $P = \sum_{k=1}^{C} P_k v_k$ virtual users. The only difference is that the symbol period of each virtual user is possibly longer than its original symbol period. The user of interest is now decomposed into v_1 virtual users; the symbols of the dth virtual user of interest are $\{b_{11}(lv_1+d)\}$. The notion of virtual users is depicted in Fig. 2. Since the original multirate problem has been converted to a single-rate problem via the decomposition into virtual users and optimal MMSE receiver for the single rate problem is time-invariant [2], [15], we immediately obtain that $u_l^\circ(t) = u_{l+v_1}^\circ(t), \forall l \in \mathbb{Z}$. The above conclusion is formally stated in the following proposition.

Proposition 1: For the C class DS-CDMA system in (1), the optimal (symbol-by-symbol) MMSE receiver for symbol l, $u_l^\circ(t)$, for Class i users is periodic with period v_i in the discrete variable l. We emphasize that the optimal receiver is a function

of two time variables, continuous variable t and discrete variable l. For each symbol, the optimal receiver changes, represented by l, and the time variation of the receiver for a fixed l is captured by t. Note that optimal receiver is periodic in l and not t.

The fact that $u_l^\circ(t)$ is periodic in l also implies that (5) is equivalent to

$$\{u_d^\circ\}_{d=0}^{v_1-1} = \arg \min_{\{u_d(t)\}} \sum_{d=0}^{v_1-1} \mathbb{E}_b \|b_{11}(kv_1+d) - \hat{b}_{11}(kv_1+d)\|^2 = \arg \min_{\{u_d(t)\}} \sum_{d=0}^{v_1-1} \mathbb{E}_b \|b_{11}(d) - \hat{b}_{11}(d)\|^2. \quad (9)$$

Note that the change in indices from $u_l^\circ(t)$ to $u_d^\circ(t)$ is done to highlight the fact that we need only v_1 unique receivers, $\{u_d^\circ\}_{d=0}^{v_1-1}$, instead of an infinite sequence of receivers, as implied by the notation $\{u_l^\circ(t)\}_{l=-\infty}^{\infty}$. For the rest of the document, we will label $u_d^\circ(t)$ as receiver for the dth virtual user of interest, $d = 0, \ldots, v_1 - 1$. Also, it is clear from the above discussion that $u_l^\circ(t) = u_d^\circ(t)$ where $d = l \bmod v_1$, i.e., the dth receiver demodulates symbol $\{b(lv_1+d)\}_{l=-\infty}^{\infty}$.

The solution to (6) was derived in [15] for the case of single-user, single-rate systems; the key steps are reproduced below for the multiuser multirate problem. For the derivation, define $Y(f), U_d(f), H(f)$ and $S_{ik}(f)$ as Fourier transform with respect to variable t of $y(t), u_d(t), h(t)$ and $s_{ik}(t-\tau_{ik})$, respectively. Also, let $V_d(f) = \mathbb{E}\{b_{11}(d)Y^*(f)\}$. Define the vector of Fourier transformed signature waveforms of all the virtual users corresponding to user ik as shown in the equation at the bottom of the page. Further define the vector of signatures of all P virtual users

$$\mathcal{Q}_k(f) = \begin{bmatrix} q_{1k}^T(f) & \cdots & q_{P_k k}^T(f) \end{bmatrix}^T_{v_k P_k \times 1}$$
$$\mathcal{Q}(f) = \begin{bmatrix} \mathcal{Q}_1^T(f) & \cdots & \mathcal{Q}_C^T(f) \end{bmatrix}^T_{P \times 1}.$$

The signature waveforms for the v_1 virtual users of interest are the first v_1 entries of the vector $\mathcal{Q}(f)$. The mean squared error, $\mathbb{E}\{|b_{11}(d) - \hat{b}_{11}(d)|^2\}$, for an arbitrary $U_d(f)$ can be written as

$$\epsilon = \int_{-\infty}^{\infty}\int_{-\infty}^{\infty} U_d^*(f)\Gamma_y(f,f')U_d(f')e^{-j2\pi(f-f')lT}\,df\,df' + \frac{N_o}{2}\int_{-\infty}^{\infty}|H(f)|^2|U_d(f)|^2\,df + 1 - 2\mathrm{Re}\int_{-\infty}^{\infty} U_d^*(f)V_d(f)\,df$$

where

$$\Gamma_y(f,f') = \frac{1}{T}\sum_{n=-\infty}^{\infty}\gamma_y^{(n)}(f)\delta\left(f-f'-\frac{n}{T}\right)$$
$$\gamma_y^{(n)}(f) = \mathcal{Q}^T(f)\mathbf{A}\mathcal{Q}^*\left(f-\frac{n}{T}\right)$$
$$V_d(f) = \mathcal{Q}^T(f)\mathcal{B}_d, \quad d = 0, \ldots, v_1 - 1.$$

The $P \times 1$ vector $\mathcal{B}_d$ is a vector of zeros except for the $(d+1)^{\text{st}}$ location which is equal to A_{11} and

$$\mathbf{a}_{ik} = A_{ik}^2\mathbf{I}_{v_k},$$
$$\mathbf{A}_k = \mathrm{diag}\,(\mathbf{a}_{1k}, \ldots, \mathbf{a}_{P_k k})_{P_k v_k \times P_k v_k},$$
$$\mathbf{A} = \mathrm{diag}\,(\mathbf{A}_1, \ldots, \mathbf{A}_C)_{P\times P}$$

where $\mathbf{I}_{v_k}$ is the $v_k \times v_k$ identity matrix. The coefficients $\gamma_y^{(n)}(f)$ can also be expressed in terms of the signature waveforms of the actual users (see Appendix A); these representations will be useful in interpreting future results. Minimizing ϵ with respect to $U_d(f)$ and using the cyclostationarity of $y(t)$, we obtain the following equation [15] to determine the optimal receiving filter for the dth virtual user:

$$\frac{1}{T}\left[\sum_{n=-\infty}^{\infty}\left[\gamma_y^{(n)}(f)\right]^* U_d^\circ\left(f-\frac{n}{T}\right)\right] + \frac{N_o}{2}|H(f)|^2U_d^\circ(f) = V_d(f). \quad (10)$$

The optimal filter admits the following form:

$$U_d^\circ(f) = \mathcal{Q}^H(f)\frac{\mathcal{G}_d(f)}{|H(f)|^2} \quad (11)$$

where $\mathcal{G}_d(f) = \mathbf{G}^{-1}(f)\mathcal{B}_d$ is a $P \times 1$ vector of periodic functions, each with period $1/T$. Under the assumption that the signature waveforms of all the virtual users are linearly independent, the $P \times P$ matrix $\mathbf{G}(f)$ is given by

$$\mathbf{G}(f) = \frac{\mathbf{A}}{T}\sum_{n=-\infty}^{\infty}\frac{\mathcal{Q}\left(f-\frac{n}{T}\right)\mathcal{Q}^H\left(f-\frac{n}{T}\right)}{\left|H\left(f-\frac{n}{T}\right)\right|^2} + \frac{N_o}{2}\mathbf{I}_P.$$

The matrix $\mathbf{G}(f)$ is positive semidefinite since both $\mathbf{A}$ and the infinite sum are positive semidefinite, and the product of two positive semidefinite matrices is also positive semidefinite [24]. Note that $U_d^\circ(f)$ is a bank of filters matched to the signature waveforms of each virtual user followed by a bank of interference suppression filters $\mathcal{G}_d(f)$ and then combining. This structure can be converted into the one with filters matched to signature waveforms of each actual user ik, followed by the following filters, $\mathcal{K}_{d,ik}(f)$ and then combining. The filters $\mathcal{K}_{d,ik}(f)$ are defined as

$$\mathcal{K}_{d,ik}(f) = \sum_{l=0}^{v_k-1}\mathcal{G}_{d,M+l}(f)e^{-j2\pi flT_k} \quad (12)$$

where $M = (i-1)P_k + \sum_{h=0}^{k-1}P_h v_h$. Note that $\mathcal{G}_{d,M+l}(f)$ represents the $(M+l)$th element of the vector $\mathcal{G}_z(f)$. The resultant filter structure for $U_d(f)$ is notionally depicted in Fig. 3, and the complete time-varying optimal solution is seen in Fig. 4.

B. Fourier Series Coefficients

In this section, we will derive the Fourier series coefficient of the optimal receiver with respect to the discrete time variable l. The derivation uses the linear independence of the user

$$q_{ik}(f) = H(f)S_{ik}(f)\begin{bmatrix}1 & e^{-j2\pi fT_k} & e^{-j2\pi f2T_k} & \cdots & e^{-j2\pi f(v_k-1)T_k}\end{bmatrix}^T_{v_k\times 1}.$$

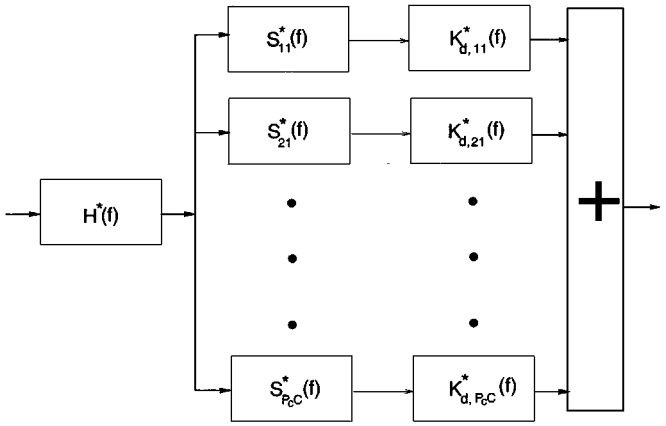

Fig. 3. MMSE receiver, $U_d(f)$, for virtual user d.

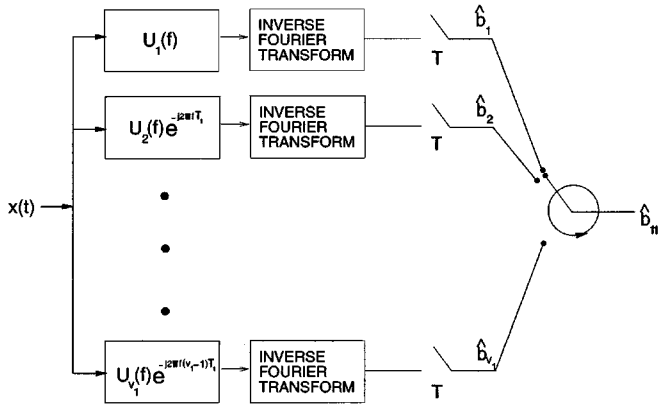

Fig. 4. Complete MMSE receiver for user 11 in the presence of multirate interference.

codes to obtain a set of linear equations in Fourier coefficients. The resultant set of linear equations can be viewed as a multichannel extension of the MMSE receiver equations for single-rate DS-CDMA systems.

In Section III-A, it was shown that the optimal linear MMSE receiver for user 11, $u_l^\circ(t)$, is cyclically time-varying in variable l with a period v_1. Thus, it admits a Fourier series expansion in the discrete time index l

$$U_l^\circ(f) = U_{l+v_1}^\circ(f) = \sum_{\alpha=0}^{v_1-1} \psi_\alpha^\circ(f) e^{-j2\pi \frac{\alpha}{v_1} l}. \tag{13}$$

Thus, $\psi_\alpha^\circ(f)$ are coefficients of a 2-D Fourier transform of $u_l^\circ(t)$. We determine the Fourier series expansion to facilitate the derivation of low-complexity receivers. Following [16], we label $(\alpha/v_1), \alpha = 0, \ldots, v_1 - 1$, as the *cycle frequencies* of the optimal MMSE receiver. Note that, instead of converting the original problem into a set of single-rate problems, we will apply the time-varying filter (13) directly to the input. This implies that the output of the filter is sampled every T_1 seconds and the symbol estimates are computed as follows:

$$\hat{b}_{11}(i) = \sum_{\alpha=0}^{v_1-1} \int Y(f) \psi_\alpha(f) e^{-j2\pi \frac{\alpha}{v_1} i} e^{-j2\pi f i T_1}\, df. \tag{14}$$

Note that $\{U_d^\circ(f)\}_{d=0}^{v_1-1}$ and $\{\psi_\alpha^\circ(f)\}_{\alpha=0}^{v_1-1}$ are isomorphic to each other. Thus, to directly compute the Fourier coefficients, $\{\psi_\alpha^\circ(f)\}$, we substitute $U_d^\circ(f)$ from (13), $d = 0, \ldots, v_1 - 1$ into (10), to obtain the following set of equations in the variables $\psi_\alpha^\circ(f)$:

$$\begin{aligned} \frac{1}{T} \Bigg[\sum_{n=-\infty}^{\infty} \left[\gamma_y^{(n)}(f)\right]^* e^{-j2\pi\left(f-\frac{n}{T}\right)dT_1} \\ \times \left(\sum_{\alpha=0}^{v_1-1} \psi_\alpha^\circ \left(f - \frac{n}{T}\right) e^{-j2\pi \frac{\alpha}{v_1} d} \right) \Bigg] \\ + \frac{N_o}{2} |H(f)|^2 e^{-j2\pi f d T_1} \sum_{\alpha=0}^{v_1-1} \psi_\alpha^\circ(f) e^{-j2\pi \frac{\alpha}{v_1} d} = V_d(f). \end{aligned} \tag{15}$$

Using the fact that $V_d(f) = e^{-j2\pi d f T_1} V_0(f)$, (15) simplifies to

$$\begin{aligned} \sum_{\alpha=0}^{v_1-1} \Bigg[\frac{1}{T} \sum_{n=-\infty}^{\infty} \left[\gamma_y^{(n)}(f)\right]^* e^{j2\pi \frac{n-\alpha}{v_1} d} \psi_\alpha^\circ \left(f - \frac{n}{T}\right) \\ + \frac{N_o}{2} |H(f)|^2 \psi_\alpha^\circ(f) e^{-j2\pi \frac{\alpha}{v_1} d} \Bigg] = V_0(f) \end{aligned} \tag{16}$$

for $d = 0, \ldots, v_1 - 1$. A weighted combination of the v_1 equations in (16) can be converted into the following set of v_1 equations. The weights used are the discrete Fourier transform coefficients $[1 e^{j2\pi(1/v_1)\beta} \cdots e^{j2\pi((v_1-1)/v_1)\beta}]$, for $\beta = 0, \ldots, v_1 - 1$:

$$\begin{aligned} \sum_{\alpha=0}^{v_1-1} \Bigg[\frac{1}{T} \sum_{n=-\infty}^{\infty} \left[\gamma_y^{(n)}(f)\right]^* \psi_\alpha^\circ \left(f - \frac{n}{T}\right) \\ \times \sum_{d=0}^{v_1-1} e^{j2\pi \frac{(n-\alpha+\beta)}{v_1} d} + \frac{N_o}{2} |H(f)|^2 \psi_\alpha^\circ(f) \\ \times \sum_{d=0}^{v_1-1} e^{j2\pi \frac{(-\alpha+\beta)}{v_1} d} \Bigg] = V_0(f) \sum_{d=0}^{v_1-1} e^{j2\pi \frac{\beta}{v_1} d}. \end{aligned}$$

Using $\sum_{d=0}^{v_1-1} e^{j2\pi(\beta/v_1)d} = v_1 \delta_\beta$, for $\beta = 0, \ldots, v_1 - 1$, the above equation reduces to the following:

$$\begin{aligned} \sum_{\alpha=0}^{v_1-1} \Bigg[\frac{1}{T} \sum_{k=-\infty}^{\infty} \left[G_x^{(kv_1+\alpha-\beta)}(f)\right]^* \psi_\alpha^\circ \left(f - \frac{kv_1 + \alpha - \beta}{T}\right) \\ + \delta_{\beta-\alpha} \frac{N_o}{2} |H(f)|^2 \psi_\alpha^\circ(f) \Bigg] = \delta_\beta V_0(f). \end{aligned} \tag{17}$$

Since $\psi_\alpha^\circ(f)$ is a linear combination of the $U_d^\circ(f)$, it is easy to verify that $\psi_\alpha^\circ(f)$ can be written in the following form:

$$\psi_\alpha^\circ(f) = \mathcal{Q}^H(f) \frac{\xi_\alpha(f)}{|H(f)|^2}, \quad \alpha = 0, \ldots, v_1 - 1 \tag{18}$$

where $\xi_\alpha(f)$ is a $P \times 1$ vector with periodic entries, each with period $v_1/T = 1/T_1$[4]. Using $\gamma_y^{(n)} = \mathcal{Q}^T(f)\mathbf{A}\mathcal{Q}^*(f-(n/T))$ and $V_0(f) = \mathcal{Q}^H(f)\mathcal{B}_0$, (17) can be rewritten as

$$\mathcal{Q}^H(f)\sum_{\alpha=0}^{v_1-1}\frac{\mathbf{A}}{T} \times \sum_{k=-\infty}^{\infty}\frac{\mathcal{Q}\left(f-\frac{kv_1+\alpha-\beta}{T}\right)\mathcal{Q}^H\left(f-\frac{kv_1+\alpha-\beta}{T}\right)}{\left|H\left(f-\frac{kv_1+\alpha-\beta}{T}\right)\right|^2} \times \xi_\alpha\left(f-\frac{\alpha-\beta}{T}\right)+\mathcal{Q}^H(f)\sum_{\alpha=0}^{v_1-1}\delta_{\beta-\alpha}\frac{N_o}{2}\mathbf{I}_P\xi_\alpha(f) = \delta_\beta\mathcal{Q}^H(f)\mathcal{B}_0, \quad \beta=0,\ldots,v_1-1. \tag{19}$$

We define

$$\mathbf{S}_r(f) = \frac{\mathbf{A}}{T}\sum_{k=-\infty}^{\infty}\frac{\mathcal{Q}\left(f-\frac{kv_1+r}{T}\right)\mathcal{Q}^H\left(f-\frac{kv_1+r}{T}\right)}{\left|H\left(f-\frac{kv_1+r}{T}\right)\right|^2}$$

to concisely write (19) as follows:

$$\sum_{\substack{\alpha=0\\ \alpha\neq\beta}}^{v_1-1}\left[\mathbf{S}_{\alpha-\beta}(f)\xi_\alpha\left(f-\frac{\alpha}{T}+\frac{\beta}{T}\right)+\left(\mathbf{S}_0(f)+\delta_{\beta-\alpha}\frac{N_o}{2}\mathbf{I}_P\right)\xi_\alpha(f)\right] = \delta_\beta\mathcal{B}_0 \tag{20}$$

for $\beta = 0,\ldots,v_1-1$. The sufficient condition required to conclude (20) from (19) is that the signature waveforms of all the virtual users are linearly independent [15]. Also it suffices to consider $f \in [0, 1/T_1]$ since both $\mathbf{S}_r(f)$ and $\xi_\alpha(f)$ are periodic with respect to f with period $1/T_1$. Furthermore, it is easy to verify that $\mathbf{S}_{v_1-r}(f) = \mathbf{S}_{-r}(f)$, a property which will be used later. Note that there are P equations for every $\beta = 0,\ldots,v_1-1$ in (20), and all $1/T$ frequency shifts of ξ_α appear in (20). To obtain v_1P equations in v_1P variables, frequency shift the βth equation in (20) by $-\beta/T$ to obtain

$$\sum_{\substack{\alpha=0\\ \alpha\neq\beta}}^{v_1-1}\mathbf{S}_{\alpha-\beta}\left(f-\frac{\beta}{T}\right)\xi_\alpha\left(f-\frac{\alpha}{T}\right) + \underbrace{\left(\mathbf{S}_0\left(f-\frac{\beta}{T}\right)+\frac{N_o}{2}\mathbf{I}\right)}_{\bar{\mathbf{S}}_0\left(f-\frac{\beta}{T}\right)}\xi_\beta\left(f-\frac{\beta}{T}\right) = \delta_\beta\mathcal{B}_0. \tag{21}$$

[4]On the other hand, $\mathcal{G}_d(f)$ is periodic with respect to f with period $1/T$, for all $d = 0,\ldots,v_1-1$.

Now each of the v_1 equations in (21) have the same frequency shifts of the v_1P unknowns which are

$$\bar{\xi}(f) = \left[\xi_0^T(f) \quad \xi_1^T\left(f-\frac{1}{T}\right)\cdots\xi_{v_1-1}^T\left(f-\frac{v_1-1}{T}\right)\right]^T_{v_1P\times 1}.$$

The equations in (21) can be rewritten in matrix form as shown at the bottom of the page. More insight about the matrix $\mathbf{\Phi}(f)$ can be gained by using the alternate representation of $\gamma_y^{(n)}(f)$ in (35) in Appendix A. The matrix (22) can be obtained in terms of $\hat{\mathcal{Q}}(f)$, augemented spreading code matrix in the frequency domain, by modifying the first v_1P_1 entries of the vectors $\xi_\alpha(f)$. The first v_kP_k entries of $\hat{\mathcal{Q}}(f)$ contain actual signature waveforms of the users in Class 1, instead of time-shifted copies as in $\mathcal{Q}(f)$; the remaining entries in $\hat{\mathcal{Q}}(f)$ are the same as those in $\mathcal{Q}(f)$. Derivation of the Fourier coefficients in terms of $\hat{\mathcal{Q}}(f)$ leads to the following equivalent form of $\mathbf{S}_r$:

$$\mathbf{S}_r(f) = \frac{\mathbf{B}_1(r)}{T}\sum_{k=-\infty}^{\infty}\frac{\hat{Q}\left(f-\frac{kv_1+r}{T}\right)\hat{Q}^H\left(f-\frac{kv_1+r}{T}\right)}{\left|H\left(f-\frac{kv_1+r}{T}\right)\right|^2}. \tag{23}$$

With this representation of $\mathbf{S}_r$, we see that the equations in (22) mimic those of the classical MMSE single-rate solution of [2]. It is also noted that, given our description of the cyclic correlation matrix, we could also develop cyclic decorrelating detectors using the methods in [25]. The function $\mathbf{B}_1(r)$ is periodic with respect to r with period v_1 and from Appendix B-II, it follows that only $\mathbf{B}_1(kv_1)$ depends on the amplitudes of the users in Class 1. This implies that, for $r > 0$, the matrix $\mathbf{S}_r(f)$ depends only the power of the interfering users from other classes. This immediately implies that as $A_{ik} \to 0, k > 1$, the matrices $\mathbf{S}_r \to 0$ for $r > 1$, leading to $\xi_\alpha(f) \to 0$ for $\alpha > 0$, i.e., the optimal receiver for the case of a single-rate signal is time-invariant.

In order to gain further understanding about the previous representations, it is useful to consider some special cases. The entries in the matrix $\mathbf{S}_r(f)$ represent cross correlations between the user signatures. Consider the single user case, i.e., $C = 1, P_1 = 1$ and $v_1 = 1$. The matrix $\mathbf{S}_0(f)$ has only one entry, $\mathbf{S}_0(f) = (A_{11}^2/T)\sum_{k=-\infty}^{\infty}(|S_{11}(f+(k/T))|^2/|H(f+(k/T))|^2)$, which is the spectrum of sampled matched filter output. If the effective signature waveform $(s_{11}(t)/h(t))$ satisfies the Nyquist criterion for intersymbol interference (ISI), then $\mathbf{S}_0(f) = T$ for $|f| \le 1/2T$ and zero otherwise [26], which implies that $\xi_0(f)$ is constant and the MMSE receiver reduces to the matched filter [26].

$$\underbrace{\begin{bmatrix} \bar{\mathbf{S}}_0(f) & \mathbf{S}_1(f) & \cdots & \mathbf{S}_{v_1-1}(f) \\ \mathbf{S}_{-1}\left(f-\frac{1}{T}\right) & \bar{\mathbf{S}}_0\left(f-\frac{1}{T}\right) & \cdots & \mathbf{S}_{v_1-2}\left(f-\frac{1}{T}\right) \\ \vdots & & & \vdots \\ \mathbf{S}_{-(v_1-1)}\left(f-\frac{v_1-1}{T}\right) & \mathbf{S}_{-(v_1-2)}\left(f-\frac{v_1-1}{T}\right) & \cdots & \bar{\mathbf{S}}_0\left(f-\frac{v_1-1}{T}\right) \end{bmatrix}}_{\mathbf{\Phi}(f)} \begin{bmatrix} \xi_0(f) \\ \xi_1\left(f-\frac{1}{T}\right) \\ \vdots \\ \xi_{v_1-1}\left(f-\frac{v_1-1}{T}\right) \end{bmatrix} = \begin{bmatrix} \mathcal{B}_0 \\ 0 \\ \vdots \\ 0 \end{bmatrix} = \bar{\mathcal{B}}$$

$$\mathbf{\Phi}(f)_{v_1P\times v_1P}\bar{\xi}(f)_{v_1P\times 1} = \bar{\mathcal{B}}_{v_1P\times 1} \tag{22}$$

Now consider the single-rate multiuser case, i.e., $C = 1, P_1 > 1$ and $v_1 = 1$. The mnth entry of the matrix, $\mathbf{S}_0(f)$, is the spectrum of the sampled mth matched filter output to the nth user signal, $\mathbf{S}_{0,mn}(f) = (A_{m1}^2/T) \sum_{k=-\infty}^{\infty}(S_{m1}(f+(k/T))S_{n1}^*(f+(k/T))/|H(f+(k/T))|^2)$. It is easy to verify the time orthogonality of the signature waveforms for users m and $n, m \neq n$ implies that $\mathbf{S}_{0,mn}(f) = 0$.

Finally consider the multirate multiuser case. If $v_i > 1$ for the user of interest, the period of the cyclostationarity of the received signal, T, is larger than T_1, thereby making the output of the matched filters a cyclostationary sequence (if sampled every T_1 seconds). Thus, there is a spectral correlation [16] between different frequency shifts of the sampled matched filter outputs, which is captured by $\mathbf{S}_r(f), r > 0$. The mnth entry of $\mathbf{S}_r(f)$ is the output spectrum of the mth virtual matched filter to the nth virtual user signal, both frequency shifted by $-r/T$, and the output sampled every T_1 seconds. Thus, the mnth entry of $\mathbf{S}_r(f)$ is the cross correlation between the frequency shifted versions of different virtual user signals. This cross correlation between frequency-shifted copies of the signals is similar to the one encountered in cyclic Wiener filtering [16]. It is the consideration of this cyclic correlation which provides the performance improvements of the current work versus our prior work [12]. Consider the case of $v_1 = 2$. The matrix (22) is

$$\begin{bmatrix} \bar{\mathbf{S}}_o(f) & \mathbf{S}_1(f) \\ \mathbf{S}_1\left(f-\frac{1}{T}\right) & \bar{\mathbf{S}}_0\left(f-\frac{1}{T}\right) \end{bmatrix} \begin{bmatrix} \xi_0(f) \\ \xi_1\left(f-\frac{1}{T}\right) \end{bmatrix} = \begin{bmatrix} \mathcal{B}_0 \\ 0 \end{bmatrix}$$

which implies

$$\xi_0(f) = \left(\bar{\mathbf{S}}_0(f) - \mathbf{S}_1(f)\bar{\mathbf{S}}_0\left(f-\frac{1}{T}\right)^{-1}\mathbf{S}_1\left(f-\frac{1}{T}\right)\right)^{-1}\mathcal{B}_0$$

$$\xi_1(f) = \bar{\mathbf{S}}_0^{-1}(f)\,\mathbf{S}_1(f)\,\xi_0\left(f-\frac{1}{T}\right).$$

Note that $\xi_1(f)$ is a function of $\xi_0(f)$.

IV. Suboptimal Receivers

For the cases where the periodicity of the optimal MMSE receiver is large, the complexity of the optimal receiver may be prohibitive, e.g., rate ratios, v_i, up to 100 [10]. Thus, it is of interest to investigate the design of a lower complexity receiver and the performance loss incurred due to the use of such receivers.

A. Low-Complexity Suboptimal Receivers

In this section, we consider reduced complexity receivers by truncating the Fourier series of the optimal receiver. The reduced complexity receiver thus has the following form:

$$U_l(f) = \sum_{\alpha\in\Omega} \psi_\alpha(f) e^{-j2\pi\frac{\alpha}{v_1}l}$$

where $\Omega = \{\alpha_1, \alpha_2, \ldots, \alpha_\lambda\} \subset \{0, 1, \ldots, v_1 - 1\}$. Note that $U_l(f) = U_{l+v_1}(f)$; v_1 may be a multiple of the actual period of $U_l(f)$. Since the reduced complexity receiver is periodic with respect to l with period v_1, the MSE cost consists of v_1 terms as in (9)

$$\{\psi_\alpha^\circ(f)\} = \arg\min_{\{\psi_\alpha(f)\}} \sum_{i=0}^{v_1-1} \mathbb{E}_b \|b_{11}(i) - \hat{b}_{11}(i)\|^2. \quad (24)$$

Note that we have chosen to change the index of summation from d to i, to emphasize the fact that $U_i(f)$ may no longer correspond to receivers for each virtual user; the subscript d is used to denote the receiver for the dth virtual user in Section III. If the cardinality of the set $|\Omega| = \lambda$ is less than v_1, the optimization (24) can no longer be decoupled as in (6). Thus, we need to perform a joint optimization to obtain $\{\psi_\alpha^\circ(f)\}_{\alpha\in\Omega}$. The derivation of the suboptimal receiver is similar to that of the optimal receiver in Section III and is given in Appendix B. The $\lambda P \times 1$ interference suppression vector $[\xi_{\alpha_1}^T(f-(\alpha_1/T)) \ldots \xi_{\alpha_\lambda}^T(f-(\alpha_\lambda/T))]^T$ can be obtained by solving (25), shown at the bottom of the page. Without loss of generality, assume $\alpha_1 < \alpha_2 < \cdots < \alpha_\lambda$. Note that (25) can be directly obtained from (22) by simply removing rows and columns corresponding to the suppressed cycle frequencies. However, it is not obvious, *a priori*, that the solution would admit this form due to the coupled nature of the cost function in (24). The above result forms the extension of reduced complexity signal separation filters in [16] to reduced complexity data demodulation, and both results are clearly evident in the 2-D Fourier domain (α, f).

If $\alpha = 0 \notin \Omega$, the MMSE optimization (24) has a trivial solution: all filters are equal to zero. This implies that, to have a useful suboptimal solution, the zeroth cycle frequency $\alpha = 0$ should always be included in the optimization for suboptimal receivers. Thus, the smallest set Ω which yields a nontrivial solution is $\Omega = \{0\}$, the time-invariant solution. Consider the case of $v_1 = 2$ for $\Omega_1 = \{0\}$ and $\Omega_2 = \{1\}$. Corresponding to the sets Ω_1 and Ω_2, the matrix (25) yields

$$\xi_0(f) = \bar{\mathbf{S}}_0^{-1}(f)\mathcal{B}_0, \quad \text{for } \Omega_1 = \{0\}$$
$$\xi_1(f) = \bar{\mathbf{S}}_0^{-1}(f)0 = 0, \quad \text{for } \Omega_2 = \{1\}.$$

Clearly, the zeroth cycle frequency must be included in Ω. We note that our prior work in [12] considered only the zeroth cycle frequency.

B. Performance Analysis

In this section, we provide the MMSE expressions for the suboptimal receivers discussed in Section IV-A; the derivation is straightforward, the reader is referred to [27] for details. The

$$\begin{bmatrix} \bar{\mathbf{S}}_0\left(f-\frac{\alpha_1}{T}\right) & \mathbf{S}_{\alpha_2-\alpha_1}\left(f-\frac{\alpha_1}{T}\right) & \cdots & \mathbf{S}_{\alpha_\lambda-\alpha_1}\left(f-\frac{\alpha_1}{T}\right) \\ \mathbf{S}_{\alpha_1-\alpha_2}\left(f-\frac{\alpha_2}{T}\right) & \bar{\mathbf{S}}_0\left(f-\frac{\alpha_2}{T}\right) & \cdots & \mathbf{S}_{\alpha_\lambda-\alpha_2}\left(f-\frac{\alpha_2}{T}\right) \\ \vdots & & & \vdots \\ \mathbf{S}_{\alpha_1-\alpha_\lambda}\left(f-\frac{\alpha_\lambda}{T}\right) & \mathbf{S}_{\alpha_2-\alpha_\lambda}\left(f-\frac{\alpha_\lambda}{T}\right) & \cdots & \bar{\mathbf{S}}_0\left(f-\frac{\alpha_\lambda}{T}\right) \end{bmatrix}_{\lambda P\times\lambda P} \begin{bmatrix} \xi_{\alpha_1}\left(f-\frac{\alpha_1}{T}\right) \\ \xi_{\alpha_2}\left(f-\frac{\alpha_2}{T}\right) \\ \vdots \\ \xi_{\alpha_\lambda}\left(f-\frac{\alpha_\lambda}{T}\right) \end{bmatrix}_{\lambda P\times 1} = \begin{bmatrix} \delta_{\alpha_1}\mathcal{B}_0 \\ \delta_{\alpha_2}\mathcal{B}_0 \\ \vdots \\ \delta_{\alpha_\lambda}\mathcal{B}_0 \end{bmatrix}_{\lambda P\times 1} \quad (25)$$

MMSE, when expressed in terms of $\psi_\alpha^\circ(f)$ takes the following form:

$$\epsilon_{\min}(\Omega) = 1 - \sum_{\alpha\in\Omega} v_1\delta_\alpha \int V_0^*(f)\psi_\alpha^\circ(f)\,df \qquad (26)$$

where $\delta_\alpha = 1$ if $\alpha = 0$ else $\delta_\alpha = 0$. From the discussion following (25), it is clear that the MSE is 1 if $0 \notin \Omega$, since $\psi_\alpha^\circ(f) \equiv 0$, for all $\alpha \in \Omega$; the same can be concluded from (26). The MSE error hence depends only on the zeroth Fourier coefficient, $\psi_0^\circ(f)$, which in turn depends on the set Ω through (25). The minimum error expression can be expressed in terms of $\{\xi_\alpha(f)\}_{\alpha\in\Omega}$ as follows (assuming $0 \in \Omega$):

$$\epsilon_{\min}(\Omega) = 1 - v_1 T \int_0^{v_1/T} \mathcal{B}_0^T \mathbf{A}^{-1}\mathbf{S}_0(f)\bar{\mathbf{S}}_0^{-1}(f) \times \left[\mathcal{B}_0 - \sum_{\substack{\alpha'\in\Omega\\ \alpha'\neq 0}} \mathbf{S}_{\alpha'}(f)\,\xi_{\alpha'}\left(f - \frac{\alpha'}{T}\right)\right] df. \qquad (27)$$

Note that the first two terms denote the MSE achieved by the optimal time-invariant MMSE receiver, and the last term is the extra reduction in the MSE achieved by introducing additional cycle frequencies.

C. Choice of Cycle Frequencies

From the discussion in the Section IV-B, it is clear that the zeroth cycle frequency should always be a member of Ω. Given a bound on the number of cycle frequencies, λ_o, which can be used, an obvious approach to find the best subset of $\{0, 1, \ldots, v_1 - 1\}$ is an exhaustive search over the possible $\binom{v_1}{\lambda_o - 1}$ cycle frequency subsets. A systematic nonexhaustive technique to choose an appropriate subset of cycle frequencies has proved to be so far elusive (see e.g., [16] and references therein).

Two heuristic methods of choosing the best subset, Ω, of a given cardinality, λ_o, are as follows. The first method requires calculating the Fourier coefficients for the optimal time-varying receiver and retaining the cycle frequencies corresponding to the strongest λ_o coefficients. This requires determining the optimal receiver, the computation of which may have prohibitive complexity. The second heuristic can be obtained by inspecting (27). Observe that the MSE contribution of each Fourier coefficient, $\epsilon_{\alpha'}(\Omega)$ can be bounded as follows:

$$\begin{aligned}\epsilon_{\alpha'}(\Omega) &\le v_1 T \int_0^{v_1/T} \|\mathcal{B}_0\|_\varrho \left|\left|\left|\mathbf{A}^{-1}\mathbf{S}_0(f)\bar{\mathbf{S}}_0^{-1}(f)\mathbf{S}_{\alpha'}(f)\right|\right|\right|_\varrho \times \left\|\xi_{\alpha'}\left(f - \frac{\alpha'}{T}\right)\right\|_\varsigma df \\ &\le v_1 T \|\mathcal{B}_0\|_\varrho \sup_{f,\alpha'\in\Omega\setminus 0} \|\xi_{\alpha'}(f)\|_\varsigma \times \int_0^{v_1/T} \left|\left|\left|\mathbf{A}^{-1}\mathbf{S}_0(f)\bar{\mathbf{S}}_0^{-1}(f)\mathbf{S}_{\alpha'}(f)\right|\right|\right|_\varrho df \\ &= \kappa \int_0^{v_1/T} |||\mathbf{J}_{\alpha'}(f)|||_\varrho\, df. \end{aligned} \qquad (28)$$

In (28)

$$\kappa = v_1 T \|\mathcal{B}_0\|_\varrho \sup_{f,\alpha'\in\Omega\setminus 0} \|\xi_{\alpha'}(f)\|_\varsigma$$

and

$$\begin{aligned}\mathbf{J}_{\alpha'}(f) &= \mathbf{A}^{-1}\mathbf{S}_0(f)\bar{\mathbf{S}}_0^{-1}(f)\mathbf{S}_{\alpha'}(f) \\ &= \mathbf{A}^{-1}\mathbf{S}_0(f)\bar{\mathbf{S}}_0^{-1}(f)\mathbf{S}_0\left(f - \frac{\alpha'}{T}\right)\end{aligned} \qquad (29)$$

where we have used the Schwarz and Holder inequality [24] such that $\varrho \ge 1$ and $(1/\varrho) + (1/\varsigma) = 1$. Here $\|\cdot\|_\varrho$ is ϱ-vector norm and $|||\cdot|||_\varrho$ is the corresponding vector induced matrix norm. The above bound on the mean-squared error contribution of each Fourier coefficient requires computation of only $\mathbf{S}_0(f)$ and choosing the cycle frequencies based on the magnitude of the norm $\int_0^{v_1/T} |||\mathbf{J}_{\alpha'}(f)|||_\varrho\, df$; hence, this technique has a lower computational complexity than truncating the Fourier series of the optimal receiver. In all our simulations, all three methods of choosing the best subset of cycle frequencies of a given size, i.e., exhaustive search, magnitude of the Fourier filters and using the induced norm in (28), led to the same solution.

V. Effect of Front-End Filter Bandwidth

In a system with multiple chipping rates, users with smaller bandwidth will potentially be provided with low-complexity (i.e., low-cost) receivers. This motivates us to investigate the effect of front-end filter bandwidth on the receiver performance, since the sampling rate is an important factor in the cost of the receiver. Clearly, if a front-end filter bandwidth is employed which is smaller than the received signal bandwidth, insufficient statistics for detection will result. It is the highest rate users' signal bandwidth that determines the received signal bandwidth. The sequel is an attempt to qualify the loss in sufficiency. Furthermore, the same analysis will also indicate the effect of the front-end filter on system capacity in terms of the number of users which can be served simultaneously. The subsequent analysis allows us to draw conclusions without having to resort to any assumptions about the correlation between user codes; for the same reason, the results in this section only provide trends.

Consider a multirate system with two user classes with symbol periods, $T_1 > T_2$, chipping rates, $T_{c_1} > T_{c_2}$ and spreading gains, L_1 and L_2. Let the number of users in each class be P_1 and P_2, respectively. We denote the front-end filter bandwidth used by B.

For demodulating the low rate users, the observation interval is T_1 and B is such that $(1/2T_{c_1}) \le B \le (1/2T_{c_2})$. The approximate number of dimensions in a signal of bandwidth B and observation interval T_1 is $2BT_1$ [28]. Each high-rate user contributes at most $\theta = \lceil (T_1/T_2) \rceil + 1$ virtual users. Thus, the total number of active users in the system is $P_1 + \theta P_2$, which is upper bounded by the maximum number of available dimensions

$$P_1 + \theta P_2 \le 2BT_1. \qquad (30)$$

Since the low-rate users may occupy less bandwidth than B, the number of low-rate users is upper bounded by L_1, i.e., $P_1 \le L_1$. Each of the θP_2 virtual users has approximately

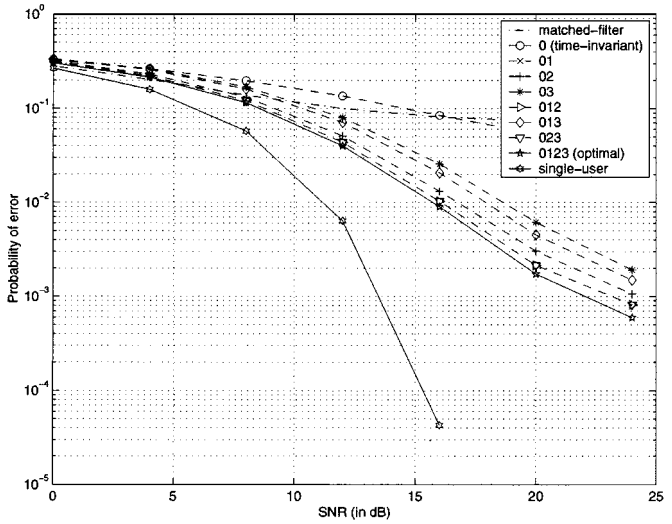

Fig. 5. Probability of error versus SNR for user 11 using the matched filter, seven suboptimal receivers with different set of cycle frequencies, and the optimal receiver; the single user bound is also given for comparison.

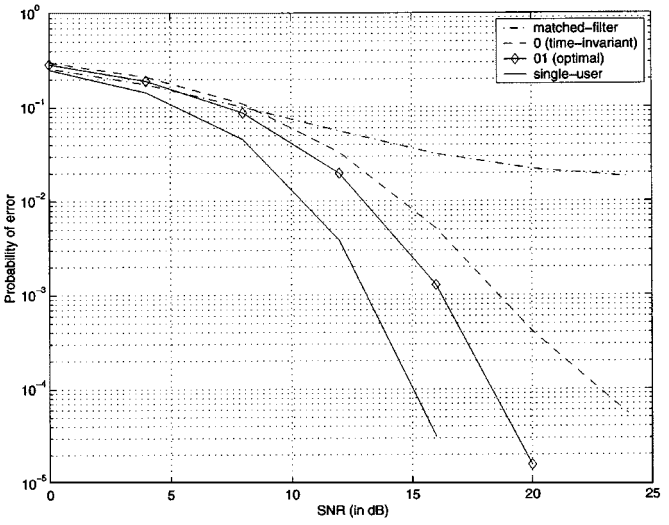

Fig. 6. Probability of error versus SNR for user 12 using the matched filter, suboptimal time-invariant receiver, and the optimal receiver; the single user bound is also given for comparison.

$L_2' = \lfloor L_2 2BT_{c_2} \rfloor$ dimensions. Combining the individual bounds on P_1 and P_2 with (30), we conclude that the feasible tuples (P_1, P_2) satisfy

$$\frac{P_1}{L_1} + \frac{\theta P_2}{L_2'} \leq 1. \tag{31}$$

Since the total number of dimensions increase with front-end filter bandwidth B, the interference suppression capability of multiuser receivers for the low rate users increases with B. Thus, increasing the bandwidth of the front-end filter beyond the low-rate user bandwidth leads an improved low-rate receiver performance for a fixed number of users, or equivalently, an increase in system capacity without loss in performance.

VI. Numerical Results

In this section, we provide representative simulation results to verify the performance of the proposed receivers. A multirate multiuser scenario in the presence of multipath is considered to compare the performance of the suboptimal MMSE receivers with the optimal MMSE receiver. Also, the front-end filter bandwidth is varied to study its effect on the receiver performance.

A. Optimal and Suboptimal Receiver Comparison

The symbol periods of the three user classes are chosen to be $T_1 = 1, T_2 = 2$, and $T_3 = 4$. The spreading gain of users in Classes 1, 2, and 3 are $L_{k_1 1} = 16, L_{k_2 2} = 32$, and $L_{k_3 3} = 32$, $k_i = 1, \ldots, P_i, i = 1, 2, 3$. With these parameters, users in Classes 1 and 2 have the same bandwidth, but different information rates. The total number of users in the system is 11, with $P_1 = 3, P_2 = 4$, and $P_3 = 4$. Further, all users in all classes have the same amplitude, $A_{ik} = 1$. The delay for each user is chosen randomly and varied from zero to two chips. Each user employs a raised cosine pulse with rolloff of 0.5, to allow a discrete time implementation. The sampling period is chosen to be $1/4$. Thus, we consider a mixed variable chipping rate, variable spreading length, single carrier system.

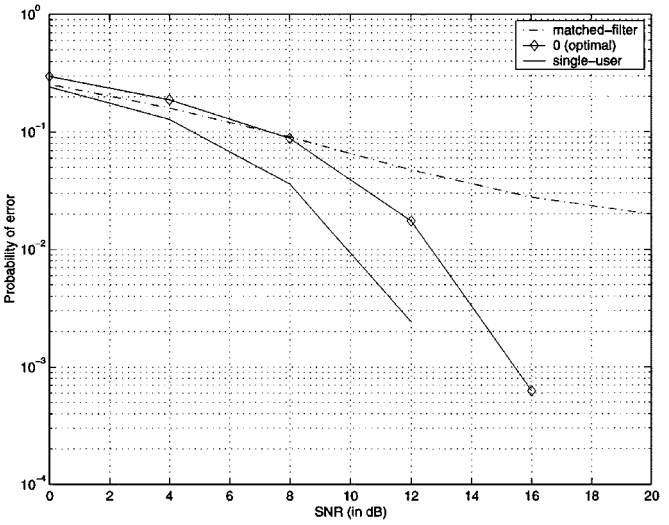

Fig. 7. Probability of error versus SNR for user 13 using the matched filter and the optimal receiver which is time-invariant in this case; the single user bound is also given for comparison.

Each user encounters a different multipath channel, which is randomly generated as follows. The delay spread of the channel is fixed, which implies that the number of taps in the discrete time representation of the channels is the same for all users because the sampling rate is the same for all users. The length of the discrete time representation of each channel is chosen to be 8, which is equal to 2 chips for Class 1, 2 chips for Class 2 and 1 chip for Class 3. The actual realization of the channel for each user is obtained by adding a random vector (independent, identically distributed with a uniform distribution on $[0, 0.1]$) to the following 8-tap channel, $[1 \quad .3 \quad .2 \quad -.15 \quad -.1 \quad -.1 \quad -.01 \quad .01]$.

The probability of error performance as a function of SNR for users 11–13 is shown in Figs. 5–7. The curves are labeled with cycle frequencies used, e.g., 013 means that the zeroth, first, and third cycle frequencies were used. The period of the optimal MMSE receiver for users in Classes 1–3 are 4, 2, and 1,

respectively; thus, the number of nontrivial suboptimal receivers obtained by using a reduced set of cycle frequencies is 7, 1, and 0, for users in Classes 1–3, respectively.

Consider the performance of user 11 in Fig. 5. From Fig. 5, it is clear that cycle frequency 2 is the most important among $\{1, 2, 3\}$. Because of the conjugate symmetry, cycle frequencies 1 and 3 can be exchanged without affecting the results. The following can be concluded from Fig. 5.

1) Each additional cycle frequency leads to improved performance. The performance increases monotonically for the sets 0, 01, 012, and 0123.
2) A smaller set of cycle frequencies may outperform a larger set of different cycle frequencies. The performance for the set 02 is better than for 013.
3) The time-invariant receiver can be considerably worse in performance than the optimal receiver, and most of the performance loss may be recoverable by a moderate increase in complexity (i.e., by including a modest number of cycle frequencies). The set 02 performs considerably better than the time-invariant receiver, and only about 2 dB away from the optimal MMSE receiver.
4) The normalized two-norm of the filter coefficients may be good predictors of suboptimal receiver performance, for example, $||\psi_l(f)||_2$, at $\mathrm{SNR} = 12$ dB, are $[1, 0.1249, 0.4150, 0.1249]$. The second cycle frequency coefficient is three times in magnitude as that of the first and third cycle frequency coefficients. The combined magnitude of $\psi_1(f)$ and $\psi_3(f)$ is less than that of $\psi_2(f)$, thereby suggesting that the cycle frequency set 02 may outperform the set 013, which is supported by the results in Fig. 5. The normalized matrix norm in (28) also follows a similar trend; they are $[1, 0.2704, 0.6024, 0.2704]$ for $\varrho = 1$ and $\varsigma = \infty$. The choice of $\varrho = 1$ and $\varsigma = \infty$ is *ad hoc* and was found to be the most accurate predictor of the performance among different values of ϱ. It is conjectured that the sup-norm ($\varsigma = \infty$) on the filter coefficients makes the inequalities tighter, leading to better estimates of the mean-squared error contributions of different filter coefficients.

B. Effect of Front-End Filter Bandwidth

The three-class case described in the previous subsection was also used to verify the effect of the front-end filter on probability of error performance. The SNR was fixed at 14 dB. For the sake of computational simplicity, the front-end filter was chosen to have a finite impulse response and its length was fixed at 20 taps.[5]

Users in Class 3 have smaller bandwidth than users in the other two classes. So, we consider the effect of the front-end filter bandwidth on the performance of the users in Class 3. The results of varying the filter bandwidth for user 13 can be seen in Fig. 8. From the figure, it is clear that the performance of the MMSE receiver improves monotonically until the front-end filter bandwidth is the same as that of the received signal. The reason for monotonic improvement in receiver performance is related to monotonic increase in number of degrees of freedom, as argued in Section V. A larger bandwidth for low-rate users in Class 3 allows the receivers to observe more dimensions of the interference from other classes, thereby leading to an improved multiaccess interference suppression.

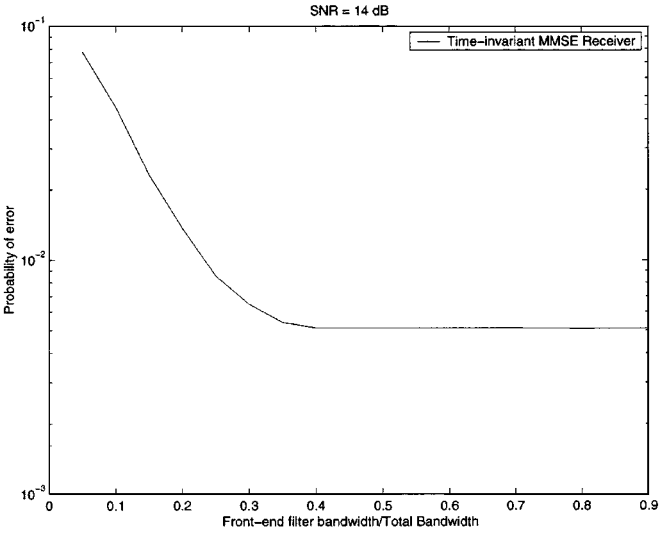

Fig. 8. Probability of error versus front-end filter bandwidth for user 13 using the optimal MMSE receiver; $\mathrm{SNR} = 14$ dB.

Thus, if out-of-rate (or out-of-bandwidth) interference is weak, the users in Class 3 can use a smaller front-end filter bandwidth, thereby reducing the computational load and hence the power consumption. This adaptive sampling technique may be useful for receiver design with strict battery power constraints.

VII. Conclusion

In this paper, we derived the optimal linear MMSE receiver for multiple data rate communications, with applications to multirate DS-CDMA and multicarrier systems. All the major results in this paper can be attributed to precise modeling of the multirate interference. Stationary models of the interference indicate time-invariant processing, leading to system performance which is strictly inferior to solutions based on the correct cyclostationary models of communication signals. Note that the additional gain from exploiting cyclostationary nature of the communication signals is accompanied with increased computational requirements. We presented a preliminary investigation of complexity performance tradeoffs with a class of low-complexity MMSE receivers. A deeper understanding of relation between computation, power, and performance at system level remains elusive.

Appendix A
Alternate Representations of $\gamma_y^{(n)}$

Two equivalent representations of $\gamma_y^{(n)}$ are derived in this section, the first in terms of actual signature waveforms of all the users and second in terms of the actual signature waveforms of users of Class 1.

[5]In practice, the front-end filter should be chosen carefully to minimize the intersymbol and co-channel interference.

A. Actual Signature Waveforms of All Users

Consider the virtual users of rate k

$$\begin{aligned}\Gamma_k(f,f') &= \frac{1}{T}\sum_{n=-\infty}^{\infty}\left[\gamma_k^{(n)}(f)\right]^*\delta\left(f-f'-\frac{n}{T}\right)\\ &= \frac{1}{v_kT_k}\sum_{i=1}^{P_k}A_{ik}^2\sum_{n=-\infty}^{\infty}v_k\mu_k(n)H(f)S_{ik}(f)\\ &\quad\cdot H^*\left(f-\frac{n}{T}\right)S_{ik}^*\left(f-\frac{n}{T}\right)\delta\left(f-f'-\frac{n}{T}\right)\\ &= \frac{1}{T_k}\sum_{n=-\infty}^{\infty}\mu_k(n)\bar{Q}_k^T(f)\mathbf{A}_k\\ &\quad\cdot\bar{Q}_k^*\left(f-\frac{n}{T}\right)\delta\left(f-f'-\frac{n}{T}\right)\end{aligned}$$

which implies

$$\gamma_k^{(n)}(f) = v_k\mu_k(n)\bar{Q}_k^T(f)\mathbf{A}_k\bar{Q}_k^*\left(f-\frac{n}{T}\right). \tag{32}$$

In (32), $\mu_k(n)$ is the indicator function which is one if v_k divides n else it is zero

$$\begin{aligned}\bar{q}_{ik}^T(f) &= H(f)S_{ik}(f)[1\quad 1\quad\cdots\quad 1]_{v_k\times 1}^T,\quad\text{and}\\ \bar{Q}_k^T(f) &= \left[\bar{q}_{1k}^T(f)\quad\bar{q}_{2k}^T(f)\quad\cdots\quad\bar{q}_{P_kk}^T(f)\right]^T.\end{aligned}$$

Define $\bar{Q}(f) = [\bar{Q}_1^T(f)\ \bar{Q}_2^T(f)\ \cdots\ \bar{Q}_C^T(f)]_{P\times 1}^T$, then we have (33) and (34), as s shown at the bottom of the page. Note that the $P\times P$ matrix $\mathbf{B}(n)$ is periodic in n with period $v = \mathrm{LCM}(v_1, v_2, \ldots, v_C)$.

B. Actual Signature Waveforms of Users in Class 1

Define

$$\hat{\mathcal{Q}}(f) = \left[\bar{\mathcal{Q}}_1^T(f)\quad\mathcal{Q}_2^T(f)\quad\cdots\quad\mathcal{Q}_C^T(f)\right]_{P\times 1}^T.$$

Following steps similar to the previous section, we obtain

$$\begin{aligned}&\gamma_y^{(n)}(f)\\ &= \hat{\mathcal{Q}}^T(f)\underbrace{\begin{bmatrix}v_1\mu_1(n)\mathbf{A}_1 & 0 & \cdots & 0\\ 0 & \mathbf{A}_2 & \cdots & 0\\ \vdots & & & \vdots\\ 0 & 0 & \cdots & \mathbf{A}_C\end{bmatrix}_{P\times P}}_{\mathbf{B}_1(n)}\hat{Q}^*\left(f-\frac{n}{T}\right)\\ &= \hat{Q}^T(f)\mathbf{B}_1(n)\hat{Q}^*\left(f-\frac{n}{T}\right).\end{aligned} \tag{35}$$

The $P\times P$ matrix $\mathbf{B}_1(n)$ is periodic in n with period v_1.

APPENDIX B
DERIVATION OF SUBOPTIMAL RECEIVER

The mean-squared error is given by

$$\begin{aligned}\epsilon(\Omega) &= 1+\sum_{i=0}^{v_1-1}\sum_{\alpha}\sum_{\alpha'}\int\int[\psi_\alpha(f)]^*\Gamma_y(f,f')\\ &\quad\times\psi_{\alpha'}(f')e^{j2\pi\frac{(\alpha-\alpha')}{v_1}i}e^{-j2\pi(f-f')iT_1}\,df\,df'\\ &\quad+\frac{N_o}{2}\sum_{i=0}^{v_1-1}\sum_{\alpha}\sum_{\alpha'}\int|H(f)|^2[\psi_\alpha(f)]^*\\ &\quad\times\psi_{\alpha'}(f)e^{j2\pi\frac{(\alpha-\alpha')}{v_1}i}\,df-\sum_{i=0}^{v_1-1}2\mathrm{Re}\\ &\quad\cdot\sum_{\alpha}\int V_i(f)\psi_\alpha^*(f)e^{j2\pi\frac{\alpha}{v_1}i}e^{j2\pi fiT_1}\,df.\end{aligned} \tag{36}$$

The optimal $\psi^\circ(f)$ should satisfy the following first-order optimality condition for $\alpha\in\Omega$:

$$\begin{aligned}&\sum_{i=0}^{v_1-1}e^{j2\pi\frac{\alpha}{v_1}i}\left[\int\Gamma_y^*(f,f')\left(\sum_{\alpha'}\psi_{\alpha'}^\circ(f')e^{-j2\pi\frac{\alpha'}{v_1}i}\right)\right.\\ &\quad\left.\times e^{-j2\pi(f-f')iT_1}\,df'+\frac{N_o}{2}|H(f)|^2\sum_{\alpha'}\psi_{\alpha'}^\circ(f)e^{-j2\pi\frac{\alpha'}{v_1}i}\right]\\ &\quad=\sum_{i=0}^{v_1-1}e^{j2\pi\frac{\alpha}{v_1}i}V_0(f)\end{aligned} \tag{37}$$

which simplifies to

$$\begin{aligned}&\sum_{\alpha'}\left[\int\Gamma_y^*(f,f')\psi_{\alpha'}^\circ(f)\sum_{i=0}^{v_1-1}e^{j2\pi\frac{(\alpha-\alpha')}{v_1}i}e^{-j2\pi(f-f')iT_1}\,df\right.\\ &\quad\left.+\delta_{\alpha-\alpha'}\frac{N_o}{2}|H(f)|^2\psi_{\alpha'}^\circ\right]=\delta_\alpha V_0(f),\quad\alpha\in\Omega.\end{aligned} \tag{38}$$

By using the cyclostationarity of $y(t)$, we obtain for $\alpha\in\Omega$

$$\begin{aligned}&\sum_{\alpha'}\left[\frac{1}{T}\sum_{n=-\infty}^{\infty}\left[\gamma_y^{(n)}(f)\right]^*\psi_{\alpha'}^\circ\left(f-\frac{n}{T}\right)\right.\\ &\quad\left.\times\sum_{i=0}^{v_1-1}e^{j2\pi\frac{(n+\alpha-\alpha')}{v_1}i}+\delta_{\alpha-\alpha'}\frac{N_o}{2}|H(f)|^2\psi_{\alpha'}^\circ\right]=\delta_\alpha V_0(f)\end{aligned}$$

$$\gamma_y^{(n)}(f) = \sum_{k=1}^{C}v_k\mu_k(n)\bar{Q}_k^T(f)\mathbf{A}_k\bar{Q}^*\left(f-\frac{n}{T}\right) \tag{33}$$

$$= \bar{Q}^T(f)\underbrace{\begin{bmatrix}v_1\mu_1(n)\mathbf{A}_1 & 0 & \cdots & 0\\ 0 & v_2\mu_2(n)\mathbf{A}_2 & \cdots & 0\\ \vdots & & & \vdots\\ 0 & 0 & \cdots & v_C\mu_C(n)\mathbf{A}_C\end{bmatrix}_{P\times P}}_{\mathbf{B}(n)}\bar{Q}^*\left(f-\frac{n}{T}\right) = \bar{Q}^T(f)\mathbf{B}(n)\bar{Q}^*\left(f-\frac{n}{T}\right) \tag{34}$$

and

$$\sum_{\alpha'}\left[\frac{1}{T}\sum_{k=-\infty}^{\infty}\left[\gamma_y^{(kv_1+\alpha'-\alpha)}\right]^*\psi_{\alpha'}^{\circ}\left(f-\frac{kv_1+\alpha'-\alpha}{T}\right)+\delta_{\alpha-\alpha'}\frac{N_o}{2}|H(f)|^2\psi_{\alpha'}^{\circ}\right]=\delta_\alpha V_0(f)$$

which is of the same form as (17). Following the computations similar to Section III-B, we obtain the following matrix equation for $\alpha\in\Omega$:

$$\sum_{\substack{\alpha'\in\Omega\\ \alpha'\neq\alpha}}\mathbf{S}_{\alpha'-\alpha}\left(f-\frac{\alpha}{T}\right)\xi_{\alpha'}\left(f-\frac{\alpha'}{T}\right)+\underbrace{\left(S_0\left(f-\frac{\alpha}{T}\right)+\frac{N_o}{2}\mathbf{I}\right)}_{\bar{\mathbf{S}}_0\left(f-\frac{\alpha}{T}\right)}\xi_\alpha\left(f-\frac{\alpha}{T}\right)=\delta_\alpha\mathcal{B}_0. \quad (39)$$

ACKNOWLEDGMENT

The authors will like to thank A. Sharma and A. Sharma of the Ohio State University for their generous help with computer simulations.

REFERENCES

[1] S. Verdú, *Multiuser Detection*. Cambridge, U.K.: Cambridge Univ. Press, 1998.
[2] U. Madhow and M. L. Honig, "MMSE inteference suppression for direct-sequence spread-spectrum CDMA," *IEEE Trans. Commun.*, vol. 42, pp. 3178–3188, Dec. 1994.
[3] E. Geraniotis, Y.-W. Chang, and W.-B. Yang, "Multi-media integration in CDMA networks," *Proc. 44th Annu. IEEE/VTS Vehicular Technology Conf.*, pp. 88–97, June 1994.
[4] M. Honig and J. B. Kim, "Allocation of DS-CDMA parameters to achieve multiple rates and qualities of service," *Proc. IEEE Globecom'96*, vol. 3, pp. 1974–1979, Nov. 1996.
[5] M. Saquib, R. Yates, and N. Mandayam, "Decision feedback detection for a dual-rate CDMA system," *ACM Wireless Networks*, vol. 4, no. 6, pp. 497–506, 1998.
[6] J. Chen and U. Mitra, "Analysis of decorrelator-based receivers for multi-rate CDMA communications," *IEEE Trans. Veh. Technol.*, vol. 48, pp. 1966–1983, Nov. 1999.
[7] J. Ma and H. Ge, "Modified multi-rate detection for frequency selective rayleigh fading CDMA channels," *Proc. 9th IEEE Int. Symp. PIMRC*, vol. 3, pp. 1304–1307, Sept. 1998.
[8] U. Mitra, "Comparison of maximum-likelihood based detection for two multi-rate access schemes for CDMA signals," *IEEE Trans. Commun.*, vol. 47, pp. 64–77, Jan. 1999.
[9] A.-L. Johansson and A. Svensson, "On multirate DS/CDMA schemes with interference cancellation," *J. Wireless Personal Comm.*, vol. 9, pp. 1–29, Jan. 1999.
[10] E. Dahlman, B. Gudmundson, M. Nilsson, and J. Sköld, "UMTS/IMT2000 based on wideband CDMA," *IEEE Commun. Mag.*, pp. 70–80, Sept. 1998.
[11] F. Adachi, M. Sawahashi, and H. Suda, "Wideband DS-CDMA for next generation mobile communication systems," *IEEE Commun. Mag.*, pp. 56–69, Sept. 1998.
[12] R. Srinivasan, U. Mitra, and R. Moses, "Design and analysis of receiver filters for multiple chip-rate DS-CDMA systems," *IEEE J. Select. Areas Commun.*, vol. 17, pp. 2096–2109, Dec. 1999.
[13] X. Wang and H. V. Poor, "Code-aided interference suppression for DS/CDMA communications. I. Interference suppression capability," *IEEE Trans. Commun.*, vol. 45, pp. 1101–1111, Sept. 1997.
[14] W. A. Gardner, "The structure of least-mean-square linear estiimators for synchronous M-ary signals," *IEEE Trans. Inform. Theory*, vol. IT-19, pp. 240–243, Mar. 1973.
[15] E. Biglieri, M. Elia, and L. Lopresti, "The optimal linear receiving filter for digital transmission over nonlinear channels," *IEEE Trans. Inform. Theory*, vol. 35, May 1989.
[16] W. A. Gardner, "Cyclic Wiener filtering: Theory and method," *IEEE Trans. Commun.*, vol. 41, pp. 151–163, Jan. 1993.
[17] L. Tong, G. Xu, and T. Kailath, "Blind identification and equalization based on second-order statistics: A time domain approach," *IEEE Trans. Inform. Theory*, vol. 40, pp. 340–349, Mar. 1994.
[18] S. Buzzi, M. Lops, and A. M. Tulino, "Blind adaptive multiuser detection for asynchronous dual rate DS/CDMA system," *IEEE J. Select. Areas Commun.*, vol. 19, pp. 233–244, Feb. 2001.
[19] A. Sabharwal, "Model Based Signal Processing for Communications and Radar," Ph.D. dissertation, The Ohio State University, Columbus, OH, Sept. 1999.
[20] A. Makagon, A. G. Miamee, and H. Salehi, *Nonstationary Stochastic Processes and Their Applications*, Singapore: World Science, 1992, pp. 147–164. ch. Periodically correlated processes and their spectrum.
[21] A. G. Miamee, "Periodically correlated processes and their stationary dilations," *SIAM J. Appl. Math.*, 1990.
[22] A. Sabharwal, U. Mitra, and R. Moses, "Cyclic Wiener filtering based multirate DS-CDMA receivers," *Proc. IEEE WCNC*, Sept. 1999.
[23] D. G. Luenberger, *Optimization by Vector Space Methods*. New York, NY: Wiley, 1969.
[24] R. A. Horn and C. R. Johnson, *Matrix Analysis*. Cambridge, U.K.: Cambridge Univ. Press, 1985.
[25] R. Lupas and S. Verdú, "Near-far resistance of multi-user detectors in asynchronous channels," *IEEE Trans. Commun.*, vol. 38, pp. 496–508, Apr. 1990.
[26] J. G. Proakis, *Digital Communications*. New York: McGraw-Hill, 1995.
[27] A. Sabharwal, U. Mitra, and R. Moses, "Low complexity MMSE receivers for multirate DS-CDMA systems," in *Proc. CISS*, Princeton, NJ, 2000.
[28] D. Slepian, "On bandwidth," *Proc. IEEE*, vol. 64, pp. 292–300, Mar. 1976.

Ashutosh Sabharwal (S'91–M'99) received the B.Tech. degree in electrical engineering from Indian Institute of Technology, New Delhi, India, in 1993 and the M.S. and Ph.D. degrees in electrical engineering from the Ohio State University, Columbus, in 1995 and 1999, respectively.

Since 1999, he has been a Post-Doctoral Research Associate at the Center for Multimedia Communication, Rice University, Houston, TX, where he is currently a Faculty Fellow. His current research interests include wireless communications, network protocols and information theory.

Dr. Sabharwal was the recipient of the 1999 Presidential Dissertation Fellowship sponsored by Ameritech.

Urbashi Mitra received the B.S. (high honors) and M.S. degrees from the University of California at Berkeley in 1987 and 1989 respectively, both in electrical engineering and computer science, and the Ph.D. degree in electrical engineering from Princeton University, Princeton, NJ, in 1994.

From 1989 until 1990, she worked as a Member of Technical Staff at Bellcore in Red Bank, NJ. From 1994 to 2000, she was an Assistant Professor in the Department of Electrical Engineering at The Ohio State University, Columbus. She became an Associate Professor in 2000 and currently holds that position in the Department of Electrical Engineering—Systems at the University of Southern California (USC), Los Angeles. At USC, she is a member of the Communication Sciences Institute and the Integrated Media Systems Center. During several occasions between 1995 and 1997, Dr. Mitra was a visiting scholar at the Institut Eurecom, in Sophia Antipolis, France.

Dr. Mitra is a recipient of a 1996 National Science Foundation CAREER award. Additionally, she has received from the Ohio State College of Engineering: a Charles E. MacQuigg Award for Outstanding Teaching in 1997 and a Lumley Award for Research in 2000. She received an NSF International Post-Doctoral Fellowship in 1994 as well as the Lockheed Leadership Fellowship (1988–1989) and the University of California Microelectronics Fellowship (1987). She serves as an Associate Editor for the IEEE TRANSACTIONS ON COMMUNICATIONS and as the Membership Chair for the IEEE Information Theory Society.

Randolph L. Moses (S'78-M'85-SM'90) received the B.S., M.S., and Ph.D. degrees in electrical engineering from Virginia Polytechnic Institute and State University, Blacksburg, in 1979, 1980, and 1984, respectively.

During the summer of 1983, he was a SCEEE Summer Faculty Research Fellow at Rome Air Development Center, Rome, NY. From 1984 to 1985, he was with the Eindhoven University of Technology, Eindhoven, The Netherlands, as a NATO Post-Doctoral Fellow. Since 1985 he has been with the Department of Electrical Engineering, The Ohio State University, Columbus, and is currently a Professor there. During 1994–1995, he was on sabbatical leave as a Visiting Researcher at the System and Control Group at Uppsala University in Sweden. His research interests are in digital signal processing, and include parametric time series analysis, radar signal processing, sensor array processing, and system identification.

Dr. Moses served on the Technical Committee on Statistical Signal and Array Processing of the IEEE Signal Processing Society from 1991 to 94. He is a member of Eta Kappa Nu, Tau Beta Pi, Phi Kappa Phi, and Sigma Xi.